AMERICAN JOURNAL OF PHYSICAL ANTHROPOLOGY 99:547–570 (1996)

Segment Inertial Properties of Primates: New Techniques for Laboratory and Field Studies of Locomotion

R.H. CROMPTON, Y. LI, R.McN. ALEXANDER, W. WANG, AND M.M. GUNTHER
Department of Human Anatomy and Cell Biology, University of Liverpool, Liverpool L69 3BX (R.H.C., Y.L., W.W., M.M.G.), and Department of Pure and Applied Biology, University of Leeds, Leeds LS2 9JT (R.McN.A.), United Kingdom

KEY WORDS Locomotion, Biomechanics, Computer Modelling, Inertia, Segment masses

ABSTRACT Studies of the dynamics of locomotor performances depend on knowledge of the distribution of body mass within and between limb segments. However, these data are difficult to derive. Segment mass properties have generally been estimated by modelling limbs as truncated cones, but this approach fails to take into account that some segments are of elliptical, not circular, cross section; and further, the profiles of real segments are generally curved. Thus, they are more appropriately modelled as solids of revolution, described by the rotation in space of convex or concave curves, and the possibility of an elliptical cross section needs to be taken into account. In this project we have set out to develop a general geometric model which can take these factors into account, and permit segment inertial properties to be derived from cadavers by segmentation, and from living individuals using linear external measurements. We present a model which may be described by up to four parameters, depending on the profile and serial cross section (circular or ellipsoidal) of the individual segments. The parameters are obtained from cadavers using a simplified complex-pendulum technique, and from intact specimens by calculation from measurements of segment diameters and lengths. From the parameters, the center of mass, moments of inertia, and radii of gyration may be derived, using simultaneous equations. Inertial properties of the body segments of four *Pan troglodytes* and a single *Pongo* were determined, and contrasted to comparable findings for humans. Using our approach, the mass distribution characteristics of any individual or species may be represented by a rigid-link segment model or "android." If this is made to move according to motion functions derived from a real performance of the individual represented, we show that recordings of resulting ground reaction forces may be quite closely simulated by predictive dynamic modelling.

Whether in the leaping of prosimians or our own bipedalism, it is impossible to achieve a full understanding of the mechanics of locomotion without a knowledge of the distribution of mass within the body and its segments: that is, their inertial properties. Thus, in leaping prosimians, as Peters and Preuschoft (1984) have pointed out, the crouching posture adopted at takeoff by specialized leapers such as *Tarsius bancanus* not only maximizes the distance over which the body center of gravity may be accelerated, but minimizes the body moment of inertia in the sagittal plane, which tends to

Received August 2, 1993; accepted September 22, 1995.

Address reprint requests to R.H. Crompton, Primate Evolution and Morphology Research Group, Department of Human Anatomy and Cell Biology, University of Liverpool, PO Box 147, Liverpool L69 3BX, United Kingdom.

rotate the body towards the pull of gravity. On the other hand, as Crompton et al. (1993) have suggested, in the more generalized leapers such as mouse lemurs, long trunks and relatively low hindlimb masses may produce moments of inertia too great to make ballistically optimal 45° takeoffs a mechanically efficient option. Inertial forces may also be useful, however: in the indriids, high forearm mass gives the forearms a moment of inertia that can be used to help rotate the body in flight (Demes and Gunther, 1989) so that long, powerful hindlimbs can be used to absorb the shock of landing.

Bipedal locomotion may be modelled as an inverted pendulum (Cavagna et al., 1977; Mochon and McMahon, 1980; Hildebrand, 1985; Winter, 1990; Preuschoft and Witte, 1991). Such locomotion therefore follows the physical laws of pendular motion, which state that while the period of a pendulum is independent of the mass of the pendulum, it is not independent of its mass distribution (Hildebrand, 1985). Thus, the distribution of mass in the limb segments can be expected to affect stride parameters. Further, as Vilensky (1979) points out, the inertia of a segment acts to resist changes in its angular motion, and is thus a determinant of its potential rapidity of oscillation. Several of the distinguishing features of the human trunk can be understood in terms of these principles (Preuschoft and Witte, 1991). For example, the greater length of the human trunk increases its inertial resistance to sagittal oscillations induced by the pendular motion of the lower limbs; while the low shoulders and broad thorax of humans increase the inertial resistance of the trunk to oscillations in the position of the center of gravity about a vertical axis. But the research utility of segment inertial properties does not stop at qualitative comparisons: as Yamazaki et al. (1979) have shown, segment inertial data together with kinematic (motion) data can be used not only to calculate the forces actually occurring during a given recorded performance (which can more accurately be measured using a forceplate), but also to predict the forces that would occur in given performances with different body proportions, so that we can actually experiment with the mechanical effects of evolutionary change.

Inertial properties are thus an essential aspect of studies of the dynamics of primate locomotion. Notwithstanding this, little effort has been made by primatologists to measure mass distribution. This neglect is certainly in part a reflection of the difficulty of gathering such data, particularly on rare or endangered species. While the properties of mass, density, and volume can readily be measured by use of balances and simple water displacement methods, several important parameters are difficult to obtain at sufficient levels of accuracy. These are the center of gravity (in essence, the mean when the distribution concerned is mass); the moment of inertia (the characteristic distribution of mass acting to resist a given angular acceleration); and the radius of gyration (essentially the standard deviation of mass distribution about the mean).

While studies of mass distribution were carried out as long ago as 1860, by Harless, the most significant and painstaking work in this field is that of Dempster (1955), who derived weights, volumes, and joint centers of rotation, used balances to calculate centers of gravity, and employed a complex-pendulum technique to calculate moments of inertia in 10 human cadavers. A variety of workers have attempted to refine these techniques and standardize method, but few have attempted to collect segment mass data from non-human primates. Grand (1977a) measured segment masses for a variety of primates and (1977b) examined segment masses in *Macaca mulatta* from a developmental perspective. However, he did not include data on centers of gravity, moments of inertia, or radii of gyration. Zihlman (1984) and Morbeck and Zihlman (1988) likewise gave segment mass proportions, but no inertial data, for *Pan paniscus, Pan troglodytes,* and *Pongo.* Reynolds (1974), however, measured masses, used the balance board technique to measure centers of gravity, and used a simple-pendulum technique to measure principle moments of inertia in *Papio cynocephalus.* Vilensky (1979) used similar techniques to obtain masses, centers of gravity, and moments of inertia in *Macaca mulatta,* also giving regression equations for predicting these parameters from body mass, and Wells and DeMenthon (1987) have de-

rived moments of inertia for *Lemur fulvus* using a rather different technique based on torsion in a bifilar (two-wire) pendulum apparatus. Their technique required two separate pieces of apparatus to measure the center of gravity (CG) and principal moments of inertia (PMI), and is not easily adopted for large primates. Sellers (1992) and Sellers and Crompton (1994) applied a geometric technique to estimation of the inertial properties of small prosimians, which is appropriate for rare museum specimens which cannot be segmented. None of these, however, have taken into account the elliptical (rather than cylindrical) nature of some segments, such as the trunk, hands, and feet, by distinguishing the moments of inertia in the u and v axes (the long and short axes of a segment of elliptical cross section; see Fig. 1).

Tardieu (1991, 1992) and Tardieu et al. (1993) offered an alternative and rather unorthodox approach to kiniesiological studies of chimpanzee and human bipedalism, which has revealed useful data about the methods used to achieve stable bipedal walking by chimpanzees. Tardieu's method used finite-element modelling to calculate the path of segment and body centers of gravity in living, moving subjects, while at the same time producing data on the three-dimensional kinematics of the limbs. Subjects were enclosed in a close-fitting body suit divided up into squares, and four orthogonally arranged motor-driven still cameras were used to record the motion and deformation of the volumes thus marked out. However, the advantage gained from being able to record the deformation of body volumes during gait, even across joints, is somewhat negated by the consequent inability to perform free-body analysis of the dynamics of individual limb segments, an essential component of standard (e.g. Winter, 1990) dynamic analysis methods. Tardieu's method also suffered from the rather large size of the cubic elements employed, in relation to limb segment volume, and from poor temporal resolution (6 frames a second), although the higher resolution of the 35 mm still camera format when compared to standard 16 mm cine or video to some extent offsets these disadvantages. The high level of subject training needed to permit use of body suits also limited detailed studies to a single, hand-reared subadult chimpanzee. Because of these limitations of Tardieu's innovative technique, it is likely that most kiniesiological studies will continue to be based on rigid-link segment models (Bresler and Frankel, 1950) in which the inertial properties are given mathematical, geometric, or physical representation. Geometric or mathematical modelling of inertial properties allows us to reduce the complexity of human and animal body shape, where multiple non-independent parameters—length, mass, center of mass, moments of inertia, and radii of gyration—must be simultaneously considered and compared.

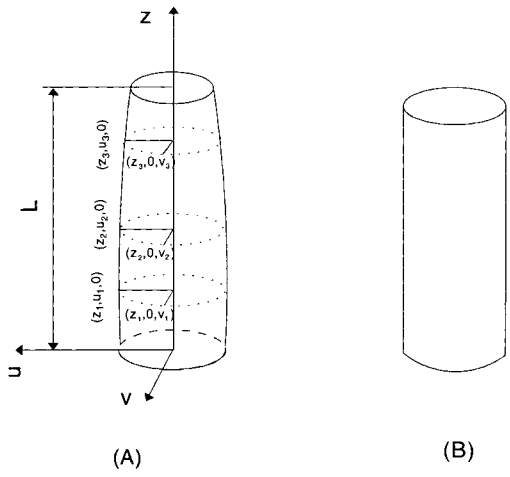

Fig. 1. Geometric models of segments. Our geometric model of each body segment **(A)** is based on a column, with either an elliptical or circular cross section. In its most general form, the cross section is an ellipse, and circular cross sections are treated as a special case of elliptical sections. The base of the column lies in the u-v plane, the long axis of the ellipse being u and the short axis v. The segment may be thought of as a solid of revolution formed by rotation of the curve of its profile about its axis, z. It can be seen that the curve depends on the radii of the cross section u and v along its length. Four parameters, k, a, b, and c, and the density ρ are needed to describe the inertial properties of a solid of revolution with an elliptical axis. They can be estimated by measuring the long and short axes of the cross section at three distances along the long axis of the segment, z_1, u_1, 0 and z_1, 0, v_1, z_2, u_2, 0 and z_2, 0, v_2; and z_3, u_3, 0 and z_3, 0, v_3, using the method detailed in Appendix 1, for which the code is provided in Appendix 2. In a rod **(B)**, the segment has a straight, not curved, outline, and parameter a has the value zero, and is not needed. If both a and b are zero, but c is non-zero, the model is a rod with a cross-sectional radius of $\sqrt{c}$.

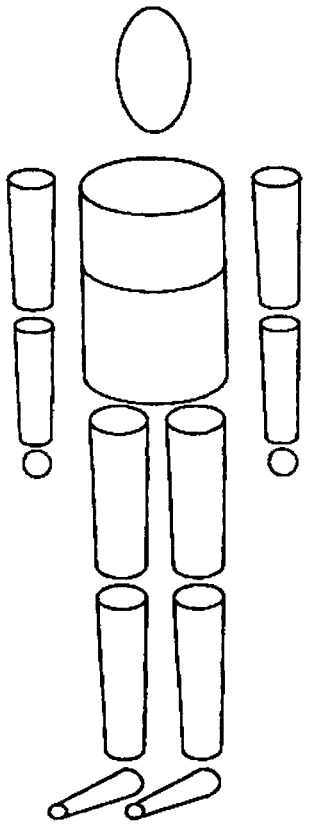

Fig. 2. The geometric inertial model of Hanavan, after Hanavan (1964). This model, based on truncated cones, does not take into account the convex or concave curvatures along the long axis of the segment.

Hanavan (1964), using conventional anthropometric data, constructed an inertial model on the basis of solid geometry (Fig. 2) where bars or truncated cones were used to represent segment geometry. The changing shape of the segment cross section along the segment (the x axis) was simply represented by circles of progressively diminishing radius. As Jensen (1978) remarked, such a model is clearly inaccurate, since segments such as the trunk, hands, and feet have an ellipsoidal, not circular, cross section, and in such a segment, we have seen that inertia will differ along the long (u) and short (v) axes of the ellipse. More recent models have not, to date, provided means of obtaining all three desired inertial parameters. That of Clauser et al. (1969) considers mass and center of mass, but not moments of inertia. A model developed by one of us (Li, 1991) succeeded in taking into consideration the center of gravity, the radius of gyration, and the convex or concave curvatures which may occur along the length of the segment (the z axis, see Fig. 1). However Li's (1991) model still failed to take into account ellipsoidal cross sections, and set segment lengths to unity.

In this paper, we have set out to develop methods which will permit segment inertial properties to be derived from cadavers by segmentation; and from living individuals using external measurements, based on a general geometric model which takes curvatures and cross-sectional shape fully into consideration, and using techniques which follow the complex-pendulum approach of Dempster (1955) and Santschi et al. (1963). The mathematical procedures involved are given in Appendix A and FORTRAN-90 source code for the calculations in the method for intact specimens is given in Appendix B.

For the first time, we report full inertial data for a sample of hominoids, and further illustrate the utility of our method by comparing forceplate records of external reaction forces during bipedal gait of a human subject with forces calculated using predictive dynamic modelling, in which motion (kinematics) derived from real performances are run through an inertial model of the subject.

METHODS

Segment model

Our geometric model of each body segment (Fig. 1A) is based on a column with either an elliptical or circular cross section. In its most general form, the cross section is an ellipse, and circular cross sections are treated as a special case of elliptical sections. The base of the column lies in the plane u-v, the long axis of the ellipse being u and the short axis v. The segment may be thought of as a solid of revolution formed by rotation of the curve of its profile about its axis, z. It can be seen that the curve depends on the radii of the cross section u and v along

its length. Four parameters, k, a, b, and c, and the density ρ are needed to describe the inertial properties of a solid of revolution with an elliptical axis. They can be estimated by measuring the long and short axes of the cross section at three distances along the long axis of the segment, z_1, u_1, 0 and z_1, 0, v_1; z_2, u_2, 0 and z_2, 0, v_2; and z_3, u_3, 0 and z_3, 0, v_3, using the method detailed in Appendix A, for which the code is provided in Appendix B. In a segment with a circular cross section, $v = u$, and since u is larger than v in the case of an elliptical cross section, the curve of the profile may also be termed u. The curve u may be described by $u = \sqrt{az^2 + bz + c}$. There are four unknowns, k, a, b, and c, where $0 < k \leq 1$, and k is the ratio of the short axis of the ellipse, v over the long axis u. If the cross section is circular, then $k = 1$, and the three unknowns a, b, and c are the only parameters necessary to describe the shape of this segment. By changing these three parameters, the inertial properties of this segment can be satisfied. But, if the cross section is elliptical, four parameters, a, b, c, and k, are required. If a is greater than zero, the profile is a concave curve; if less than zero, convex (Fig. 1A). In a rod (Fig. 1B), the segment has a straight, not curved outline, and parameter a has the value zero, and is not needed. If both a and b are zero, but c is non-zero, the model is a rod with a cross-sectional radius of $\sqrt{c}$.

Subjects

Four common chimpanzees (*Pan troglodytes*), two adult female, one adult male, and one juvenile male, and one juvenile orangutan (*Pongo pygmaeus*) were used for this study. These specimens were captive-bred individuals, obtained after death from natural causes at the North of England Zoological Society's Chester Zoo. The specimens had been kept on large, open islands with ample room and facilities for exercise. They did not exhibit any muscle wasting or other visible musculoskeletal abnormality. One *Pan, Pan* 2, was frozen shortly after death, and the other three specimens fixed in formol alcohol by perfusion and kept in tanks filled with methyl alcohol. The specimen of *Pongo* was perfused and then held frozen.

Segmentation

For the purposes of this study, the body was divided into the following segments: 1) head (with neck); 2) torso; 3) upper arm; 4) forearm; 5) hand; 6) thigh; 7) leg; 8) foot. These segments were chosen as those readily recognizable when analyzing film records, and form the links of our rigid-segment model. Segmentation may be done either frozen, by sawing, or unfrozen, by dissection. Dempster (1955) froze his specimens with the joints fixed at the angle midway through the range of motion of the joint concerned, and then sawed through the frozen limb at the approximate position of the center of rotation of the joint. His technique has the advantage that muscle is more readily assigned to its biomechanically correct segment. Segmentation by dissection of unfrozen cadavers suffers from the possibility of distortion of unfrozen muscle under gravity. However, primate cadavers are in our view too valuable to permit extensive sawing. Therefore, noting that there is no single ideal method of segmentation, we have adopted careful dissection of unfrozen specimens, cutting them so that muscle is divided between segments in a plane, sometimes curvilinear, passing through the estimated joint center. Whenever the fixation conditions permitted, the cut was made with a joint in the midposition of its approximate normal range of motion, for the plane of motion in which the largest joint excursion occurs, as in Dempster (1955).

The segments were removed by careful dissection using a scalpel, a saw being used only to cut through vertebral bodies when the scalpel cut did not correspond to the position of the intervertebral disc. Great care was taken during dissection to prevent distortion of the specimen under gravity, and the specimens were frozen, supported against gravity, immediately after separation, to prevent later distortion.

Two *Pan* were segmented on both sides, so that techniques could be practised and verified before data were retained. The trial segmentations were recorded on videotape, so that subsequent segmentations could be made in as identical a manner as possible.

The divisions between segments were

made according to functional/mechanical criteria rather than by section along a plane, thus:

a) The head and neck were severed in a curve with its convexity facing into the trunk, just about the "vertebra prominens," which marks the transition in the general direction of the inclination of the vertebral spines from anteroposterior to craniocaudal, laterally on either side to a point level with the superior margin of the glenoid fossa and anteriorly to a point just above the nearest approximation of the clavicles.

b) The upper arms were severed in a curve cutting through the anterior and posterior muscular walls of the axilla with the arm held in a semi-abducted posture, meeting the humeral head so that half of the convexity was included in the arm segment, and half free. The cut was continued superiorly to the tip of the acromion process, and posteriorly and anteriorly to meet the cut through the axilla.

c) The upper arm was separated from the forearm by a cut tracing the olecranon process, so that all of the triceps was included in the upper arm, and the cut continued laterally and anteriorly in the plane of the radiohumeral articulation, with the elbow held at 90°.

d) The forearm was separated from the hand by an incision distal to the radial and ulnar styloid processes, returning proximally to the plane of the radiocarpal articulation.

e) The thigh was separated from the torso by a curving incision through the gluteal musculature just proximal to the greater trochanter, exposing the femoral head posteriorly and dividing the hip muscles so that the head was approximately 50% free, the cut being continued anteriorly and inferiorly in this plane to meet the posterior incision through the adductor muscles.

f) The thigh was separated from the leg by an incision begun laterally in the plane of the tibial plateau, proximal to the menisci, with the knee at 90°, continuing anteriorly just distal to the patella, so that 50% of the curvature of the femoral condyles was free.

g) The foot was separated from the leg by an incision begun anteriorly in the plane of the talocrural joint, continued laterally and medially following the margins of the malleoli, and returning to the plane of the talocrural joint by incision through the Achilles tendon.

The segmented specimens were weighed immediately using an Ohaus CT 6000 S electronic balance (range 0–6,000 g, accurate to 1 g); and a Soehnle Digital S electronic balance (range 0–130 kg, accurate to 100 g) for specimens over 6,000 g in weight.

Segment mass density

Density measurements were made for the limb segments and head of frozen specimens *Pan* 2 and *Pongo:* the latter had been perfused before freezing. Evisceration made such measurements on the trunk impossible. Since immersion in alcohol was judged certain to affect density, no attempt was made to measure the density of specimens *Pan* 1, *Pan* 3, and *Pan* 4. The segments were weighed immediately prior to measurement. A cylindrical tank was filled to the brim with water, and the specimen lowered into the tank. Displaced water running from the lip of the tank was collected in a graduated cylinder, and the volume displaced was recorded as soon as water ceased to flow. Volumes were measured using Dempster's (1955) method and densities then calculated as mass/volume. The segment mass density (mass/displaced volume) is recorded in Table 1.

Centers of gravity, principal moments of inertia, and radii of gyration

For cadavers, the data required for calculation of inertial properties by segmentation could in all cases but the trunk be measured with a high degree of accuracy using a complex-pendulum technique. In this, we measure the number of swing cycles completed by a segment-frame assembly about two parallel axes in a given time.

Two frames, as shown in Figure 3, but of different sizes, were constructed, with fixing screws (F in Fig. 3) to hold the specimen, and the frames were drilled through in two locations of known distance d from each other, for the passage of a thin stainless steel rod about which the whole frame/specimen assembly was swung. The mass of the empty frame was measured precisely before em-

TABLE 1. Inertial characteristics of Pan *and* Pongo *measured in this study*

Segment	Mass (g)	CG (%)	RG_{xx} (%)[a] (mediolateral)	RG^{a}_{yy} (%)[a] (sagittal)	Length (mm)	Mass density (g/cm^3)
Pan 1						
Trunk (entire)	18200	219.0 (45.0)	155.8 (32.0)	160.4 (32.9)	487	—
Trunk −abd. v.	7200	237.0 (48.7)	166.0 (34.1)	170.4 (35.0)	—	—
Trunk −viscera	12300	229.0 (47.0)	167.9 (34.5)	173.2 (35.6)	—	—
Upper arm	1281	113.9 (44.5)	78.6 (30.1)	—	256	—
Forearm	935	136.3 (50.5)	75.0 (27.8)	—	270	—
Hand	332	70.0 (46.4)	47.8 (31.7)	50.0 (33.1)	151	—
Thigh	2249	108.0 (42.9)	84.0 (33.0)	—	252	—
Leg	908	133.2 (52.2)	65.8 (25.8)	—	255	—
Foot	554	63.2 (35.1)	46.1 (25.6)	—	180	—
Pan 2						
Head	3054	106.0 (41.7)	70.3 (27.7)	—	245	1.067
Trunk (est.)	—	—	—	—	588	—
Trunk −viscera	18900	215.6 (36.7)	223.2 (38.0)	234.5 (39.9)	—	—
Trunk −s. sw.	16000	274.3 (46.6)	189.0 (32.1)	196.0 (33.3)	—	—
Upper arm	2137	130.0 (45.8)	86.7 (35.5)	—	284	1.069
Forearm	1642	144.4 (47.2)	80.4 (26.3)	—	306	1.074
Hand	616	98.7 (43.7)	61.9 (29.1)	25.1 (29.9)	226	1.11
Thigh	3270	113.7 (40.9)	82.7 (29.7)	—	278	1.037
Leg	1382	153.7 (54.7)	77.7 (27.7)	—	281	1.08
Foot	712	71.4 (33.5)	54.3 (25.5)	—	213	1.09
Pan 3						
Head	787	61.7 (43.2)	42.6 (29.8)	—	143	—
Trunk −viscera	1397	125.6 (49.4)	82.7 (32.6)	89.6 (35.3)	254	—
Upper arm	145	55.7 (48.8)	35.0 (30.7)	—	114	—
Forearm	159	58.9 (49.3)	32.6 (27.3)	—	120	—
Hand	43	35.9 (42.8)	24.1 (26.7)	25.1 (29.9)	84	—
Thigh	219	45.6 (40.0)	35.1 (30.8)	—	114	—
Leg	109	58.9 (51.2)	30.7 (26.7)	—	115	—
Foot	61	44.7 (50.8)	23.0 (26.1)	—	88	—
Pan 4						
Head	5025	97.1 (45.6)	76.2 (35.8)	—	213	—
Trunk −viscera	26800	253.4 (50.7)	131.0 (26.2)	151.5 (30.3)	500	—
Upper arm	2564	118.8 (50.8)	74.0 (31.6)	—	234	—
Forearm	2032	110.1 (43.7)	70.6 (28.0)	—	252	—
Hand	805	67.8 (37.2)	52.6 (28.9)	53.3 (29.3)	182	—
Thigh	4351	114.4 (44.9)	79.8 (31.3)	—	255	—
Leg	2083	113.0 (48.1)	66.6 (28.3)	—	235	—
Foot	807	69.2 (37.2)	50.9 (27.4)	—	186	—
Pongo						
Head	2938	124.0 (60.0)	64.0 (30.9)	—	207	1.116
Trunk −viscera	5332	195.5 (47.9)	142.3 (34.9)	146.7 (36.0)	515	—
Upper arm	920	109.5 (47.0)	80.5 (34.5)	—	233	1.062
Forearm	836	142.2 (55.3)	72.0 (28.0)	—	257	1.105
Hand	448	73.2 (44.9)	54.9 (33.7)	52.9 (32.5)	163	1.05
Thigh	1070	79.1 (46.3)	59.9 (35.0)	—	171	1.05
Leg	686	93.8 (48.6)	57.6 (29.8)	—	193	1.04
Foot	528	69.7 (36.9)	54.2 (28.7)	—	189	1.03

[a] Except for the hand and trunk, the RG_{yy} of segments are assumed equal to RG_{xx}. The y axis is sagittal, the x axis coronal. Trunk −viscera = trunk minus all viscera; trunk −abd. v. = trunk minus abdominal viscera, etc. (est.) = intact mass, estimated by technique given in the text. The positions of the center of gravity are normally distances of the center of gravity from the proximal joint center, expressed as percentages of segment length. In the case of the feet, trunk, and head, the proximal joint center does not, of course, correspond to the proximal end of the segment. The centers of gravity of the foot, trunk, and head are thus defined with reference to the calcaneal tuberosity, center of the acetabulum, and extemal occipital protuberance.

ployment using a standard laboratory balance and its swing period about the axis rod, balanced on knife-edges, was calibrated using a stopwatch accurate to 0.01 second. The segments were mounted in the frame appropriate to their size and clamped securely. Trials indicated that the repeatability of measurements made on unfrozen specimens was poor, as fluid and/or tissue was displaced under gravity. To prevent this, the specimen together with the frame (but without the axis rod) was refrozen overnight, in a chest freezer, carefully supported against deformation, immediately after the specimen was mounted, in order to render the entire frame/specimen assembly as rigid as possible. The

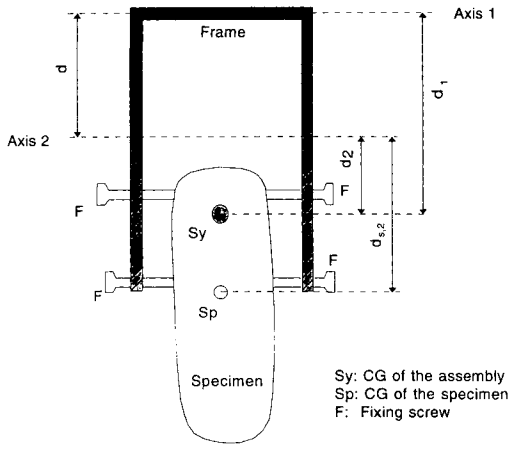

Fig. 3. Schematic drawing of the complex-pendulum frame used in this study, together with distances (d) measured and used in the text equations. The frame/specimen assembly was swung on a stainless-steel rod, balanced on a knife edge, at axis 1 and axis 2, and the period of the complete assembly, swinging about these axes, was measured to derive information about the mass distribution of the specimen. Abbrevations: axis 1, location of first axis; axis 2, location of second axis; d, distance between axis 1 and axis 2; d_1, distance between axis 1 and the CG of the assembly (Sy); d_2, distance between axis 2 and the CG of the assembly (Sy); d_{s2}, distance between axis 2 and the CG of the specimen (Sp); F, position of screws for fixing specimen to frame.

assembly was weighed immediately before being swung, and, without being removed from the freezer, swung with the axis rod in each position (axis 1 and axis 2, Fig. 3), balanced on a pair of polished stainless steel edges (knife-edges were used for smaller specimens). The time taken for the specimen and frame assembly to complete 50 swing cycles was recorded. This experiment was repeated three times, for each axis position, and the mean time for each position recorded. These data were then used to calculate the inertial properties and model parameters using the method detailed in Appendix A.

Most limb segments can safely be assumed to have equal moments of inertia and radii of gyration in the v and u directions (i.e., orthogonally different diameters). While the shape of the proximal limb segments is such that v and u planes will have very similar inertial values (Chandler et al., 1975), this is not so for the trunk and hands, and in these cases, therefore, we swung these specimens in the two planes to derive the inertial properties in each direction. The feet of these specimens were judged likely to have very similar inertial values in the two directions, and only one value is given.

Method for the trunk

While, in the case of the trunk, exactly the same technique could be applied, we did not have the technical facilities to build an equally accurate frame of adequate size, and a different method was adopted. A balance-board technique derived from Contini (1972) was employed to derive the location of the center of gravity with reference to the center of the acetabulum. The torso was frozen and two holes were drilled through the pelvis at right angles. A strong stainless-steel rod was passed through each hole in succession and the moment of inertia determined for the v and u planes by a single set of swings in each direction.

Prediction of ground reaction forces from inertial and kinematic data

Ground reaction forces occurring during normal human bipedal walking were compared to simulated forces calculated for motion of an inertial model of a randomly selected subject by predictive dynamic modelling (see, e.g., Haug, 1989). The latter technique requires construction of a rigid-link segment model, which treats the body as being made up of a number of segments, linked by joints of given ranges of mobility, and given appropriate inertial properties (mass distribution). Each link can be considered in isolation, and, given a knowledge of segment inertial properties, the internal or external forces acting upon it can be calculated from a knowledge of its motion. The external forces must originate from either the external environment or neighboring links. Thus, working out sequentially along each limb, the ground reaction force may be estimated. Actual ground reaction forces for normal bipedal walking of the subject were measured using a Kistler 9281B11 forceplate set flush with a 12-m wooden runway as described in Crompton and Li (in press). Segment motion

(angular and linear accelerations and velocities [i.e. kinematics]) was recorded synchronously using two orthogonal genlocked CCD video cameras, and reconstructed in 3-D using our own software, GAP (Sellers and Crompton, 1994). Then, a rigid-link computer model (android) of the subjects' dimensions and inertial properties of the subject was constructed using the preprocessor of a standard commercial dynamic modeller, ADAMS/Android (MDI Inc., 1992) on the basis of anthropometric measurements and the Chandler et al. (1975) database. Standard ranges of joint mobility, and appropriate levels of compliance and damping at joints, were utilized. Motion curves describing the linear and angular accelerations and velocities of the subject's segments (derived from the kinematic recordings) were then used to drive the computer representation of the subject using ADAMS/Solver (MDI Inc., 1992), and the forces necessary at each joint to bring about these kinematics, given the inertial properties of the model, were then calculated. Working out from the body center of gravity to the sequential ground-subject contact points the resulting ground reaction forces could then be calculated by the methods detailed in Haug (1989) and Winter (1990).

RESULTS

Five trials of the complex-pendulum technique were made using an artificial limb segment (part of a shop display dummy) of mass 845 g in a frame of mass 145 g. These produced principal moments of inertia (PMIs) with a coefficient of variation of 0.46%. The radii of gyration had a coefficient of variation of 0.23%. The mass, mass densities, centers of gravity, and radii of gyration of the segments of each specimen studied in this project are given in Table 1. The principal moment of inertia (PMI) is simply the product of the mass and the square of the radius of gyration, which are reported here as independent parameters. The PMI is therefore not listed.

Density measurements of *Pan* 2 produced the result predicted by Dempster (1955): the more distal segments have progressively higher density. However, the *Pongo* results are less satisfactory in the latter respect, suggesting that any perfusion previous to freezing may change the density properties of limb segments.

Our own sample size is necessarily small, as our material is, of course, limited to that provided by natural deaths of captive animals. However, we present the parameters of the inertial models created in this study in Table 2, together with values for six adult male human cadavers calculated from Chandler et al. (1975), which is the study most directly comparable with our own. Where the data were sufficient, and the results thought reasonable reliable, we also present parameters calculated from Reynolds' (1974) study of four female *Papio,* Vilensky's (1979) male and female means for *Macaca mulatta,* and Wells' and De Menthon's (1987) study of a single *Lemur fulvus.* Figure 4 gives a graphic representation of the inertial models of *Pan* 1, *Pan* 2, *Pan* 4, and *Pongo* 1. In Table 3, mass proportion data are presented together with data on three children from Jensen (1987), Zihlman (1984) on *Pan paniscus,* and Morbeck and Zihlman (1988) on two *Pongo* (*Pongo* 2 and *Pongo* 3).

Figure 5 shows simulated vertical and sagittal (or fore-aft) reaction forces between the foot and ground during the stance phase in comparison to those actually recorded by the Kistler forceplate during the same phase in the real performance. It can be seen that the real forces are well predicted, but the magnitude and sharpness of the peaks and troughs of the curves are sometimes different in the two sets of curves.

DISCUSSION

The inertial characteristics (Table 1) of hominoids measured in this study bear closest comparison with the work of Chandler et al. (1975) on human cadavers. The mean position of the center of gravity (CG) of the upper arm is more proximal in *Pan* (44.5% and 46.6% for the two females, and 47% for the infant *Pongo,* but 50.8% for the adult male *Pan*) than it is in humans, where Li and Dangerfield (1993) found that the CG becomes progressively more proximal in children of increasing age. The forearm, on

TABLE 2. Parameters of dynamic models for limb segments

Code	k	a	b	c	L (cm)
Head					
Pan 1	—	—	—	—	—
Pan 2	1	−0.15365	2.496	37.2	25.4
Pan 3	1	−0.17023	1.490	17.4	14.3
Pan 4	1	0.18890	−5.768	103.2	21.3
Pongo 1	1	−0.07462	3.891	10.86	20.7
Trunk					
Pan 1	0.8025	0.12374	−7.852	241.6	48.7
Pan 2	0.7325	0.01133	−2.551	236.9	58.8
Pan 3	0.3451	0.28505	−7.384	83.21	25.4
Pan 4	0.5622	−0.5538	28.20	59.96	50.0
Pongo 1	0.5737	0.11928	−7.015	160.26	51.5
Upper arm					
Pan 1	1	0.01794	−0.8433	21.78	25.6
Pan 2	1	0.02170	−1.0140	30.97	28.4
Pan 3	1	0.01965	−0.0272	4.485	11.4
Pan 4	1	0.01793	−0.2856	32.70	23.4
Pongo 1	1	0.11846	−2.943	24.68	23.3
Human 1	1	0.013726	−0.2979	20.27	28.2
Human 2	1	0.015585	−0.5670	24.12	30.5
Human 3	1	−0.011354	0.3138	22.08	29.1
Human 4	1	0.040627	−0.0723	18.57	29.8
Human 5	1	0.008895	−0.02964	14.75	26.7
Human 6	1	0.018480	−0.6256	22.28	27.6
Macaca[1]	1	−0.0079683	−0.01150	6.47	12.6
Lemur	1	−0.079100	0.6272	1.06	8.5
Papio	1	−0.083147	1.4368	1.82	17.7
Forearm					
Pan 1	1	−0.02437	0.6799	6.999	27.0
Pan 2	1	−0.05476	1.5010	10.03	30.6
Pan 3	1	−0.07943	0.9215	2.219	12.0
Pan 4	1	0.07469	−1.1653	25.03	25.2
Pongo 1	1	−0.01484	0.6133	4.757	25.7
Human 1	1	0.033783	−1.3689	21.33	26.6
Human 2	1	−0.0004565	−0.3932	17.63	29.4
Human 3	1	0.0086180	−0.9181	25.81	24.9
Human 4	1	0.031387	−1.2155	18.06	25.4
Human 5	1	0.017467	−0.8661	17.75	25.3
Human 6	1	−0.016514	0.11813	14.46	26.1
Macaca[1]	1	0.0032891	−0.2634	4.88	14.0
Papio	1	0.0019581	−0.2382	6.12	21.3
Head					
Pan 1	0.5551	0.12922	−2.2761	18.72	15.1
Pan 2	0.3640	−0.04355	0.2660	25.88	22.6
Pan 3	0.2819	−0.113644	0.4167	6.129	8.40
Pan 4	0.9039	0.047106	−2.0416	27.41	18.2
Pongo 1	0.6401	0.17089	−3.274	24.57	16.3
Macaca[2]			No solution for the equations		
Thigh					
Pan 1	1	0.15806	−4.909	55.79	25.2
Pan 2	1	−0.01392	−1.226	61.71	27.8
Pan 3	1	0.070132	−1.421	10.96	11.4
Pan 4	1	−0.051823	0.06449	62.78	25.5
Pongo 1	1	0.26349	−4.998	36.02	17.1
Human 1	1	0.066845	−3.623	79.28	40.5
Human 2	1	0.073989	−4.558	106.2	44.4
Human 3	1	0.10878	−6.318	137.1	41.0
Human 4	1	0.10681	−5.833	91.31	44.4
Human 5	1	0.18190	−8.513	119.7	37.4
Human 6	1	0.16450	−7.621	108.9	37.1
Macaca[1]	1	−0.064064	1.0203	5.90	14.7
Lemur 3	1	−0.067226	1.084	0.91	13.1
Papio	1	−0.0086155	−1.5018	20.5	20.3

(*continued*)

TABLE 2. Parameters of dynamic models for limb segments (continued)

Code	k	a	b	c	L (cm)
Leg					
Pan 1	1	−0.060000	1.6387	2.607	25.5
Pan 2	1	−0.03032	1.1429	6.417	28.1
Pan 3	1	−0.12459	1.4891	1.287	11.5
Pan 4	1	0.12991	2.799	17.15	23.5
Pongo 1	1	−0.0087034	0.07328	11.25	19.3
Human 1	1	0.011923	−0.9001	29.06	38.1
Human 2	1	0.011329	−0.9509	33.42	45.7
Human 3	1	−0.0020762	−0.6684	41.22	40.6
Human 4	1	0.035405	−1.8474	32.76	39.7
Human 5	1	0.0066464	−0.5897	24.99	42.4
Human 6	1	0.01012	−0.8454	27.43	41.6
Macaca[1]	1	−0.0063360	−0.09333	5.16	15.9
Lemur	1	−0.017557	0.3498	0.11	12.4
Papio	1	−0.0043769	−0.1453	6.64	19.3
Foot					
Pan 1	1	−0.021853	−0.4988	15.84	18.0
Pan 2	1	0.0068830	−1.0540	19.95	21.3
Pan 3	1	−0.103734	0.93577	0.58	8.8
Pan 4	1	−0.01874	−0.6978	21.32	18.6
Pongo 1	1	0.038394	−1.444	17.71	18.9
Human 1	1	−0.02228	0.9344	3.52	23.0
Human 2	1	−0.071963	2.114	1.12	25.3
Human 3	1	−0.066561	1.925	1.66	22.9
Human 4	1	−0.054389	1.497	1.18	23.5
Human 5	1	−0.042022	1.247	2.49	22.5
Human 6	1	−0.051755	1.495	0.02	23.1
Macaca[1]		No solution for the equations			

[1] *Macaca* data pool males and females.

the other hand, shows the opposite pattern, with the female *Pan* and *Pongo* having a CG located more distally than in humans, at about the midpoint, while the human CG is located at around 42% of the way along the forearm. Once again the male has a CG close to that of humans, at 43% of forearm length. The CG of the human thigh, on the other hand, located at 40% of its length, is not dissimilar to the female *Pan* and the *Pongo,* but in this case the male differs with a more distal CG (45%). In the leg (crus), the human CG is again more proximal, at 42% of its length. In all the other hominoids, the CG of the leg is either near the midpoint or distal to it. A pattern for reduction in mass of the middle segment in humans, taken together with the fact that the hands and to a lesser extent the feet of *Pongo* and *Pan* form a larger percentage of total body mass than they do in adult humans, indicates a generally more distal concentration of mass in apes. Our findings thus agree to some extent with the theoretical results of Preuschoft and Witte (1991) and Preuschoft et al. (1992), who indicated that humans would be expected to have a more proximal location of the lower-limb CG than the apes, since that would reduce the inertial resistance of the limb to pendular motion. On the other hand, a more proximal CG in the human upper limb is not so clearly predicted by Preuschoft and co-workers, who refer rather to a conservation of moderate mass and length in humans serving to match the resonant frequency of the upper and lower limbs, and so permitting compensation for the rotations set up in the upper body by the swinging of the legs. However, Tardieu (1991, 1992) has demonstrated that the stability of the path of the human CG is a consequence of the synchronization of vertical and horizontal oscillations of the trunk. In the absence of such synchronization, chimpanzees are still able to achieve stability of the path of the whole-body CG (contra Jenkins, 1972) by compensatory movement of the arms and, to a lesser extent, the upper body, in a manner not dissimilar to that adopted by human tightrope walkers. The efficacy of the arms in this respect would indeed be increased by a more distal CG. However a distal CG in the arms of chimpanzees (and hence a larger moment of inertia about the proximal joint)

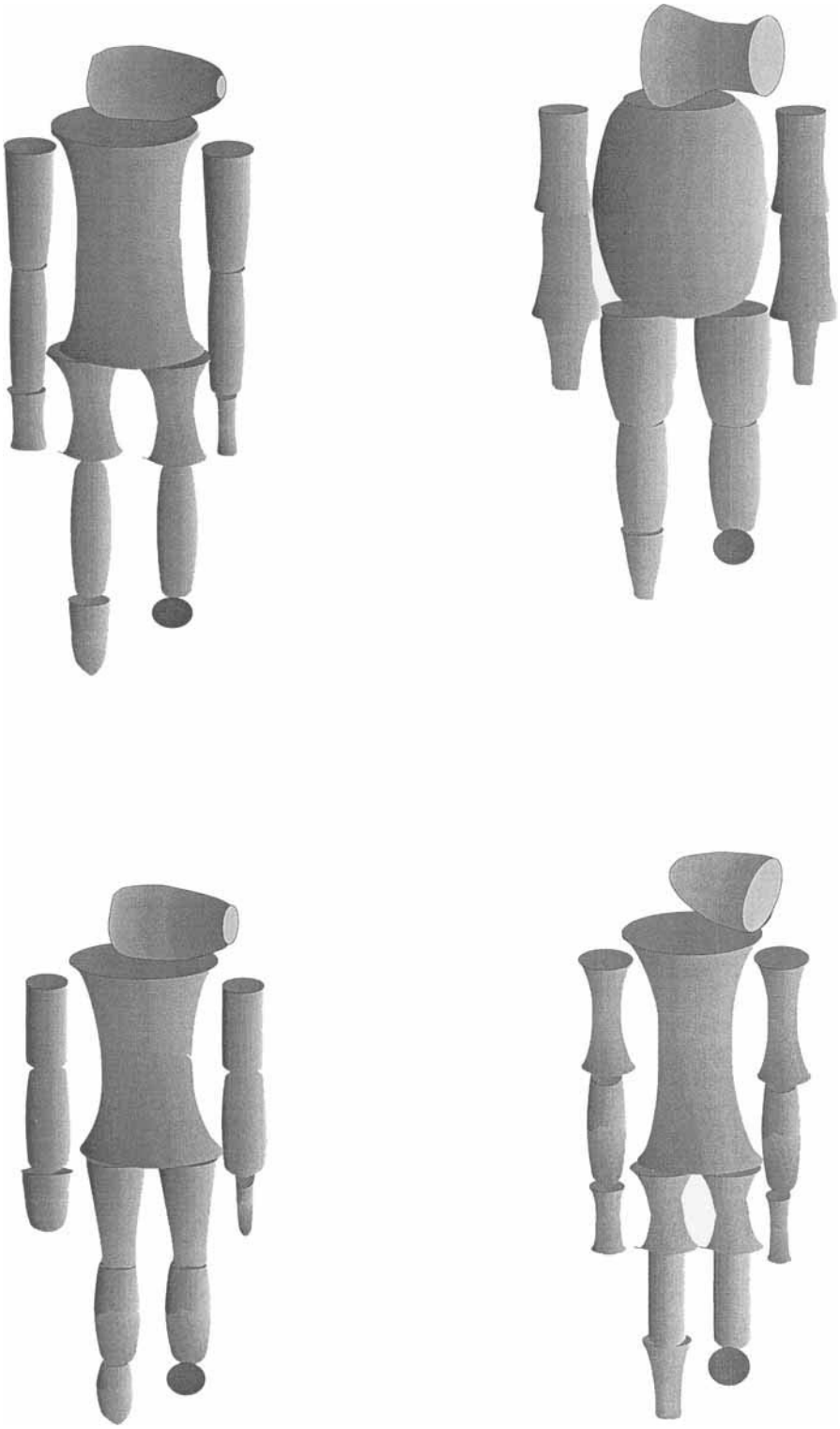

Fig. 4. Three-dimensional inertial models of *Pan* 1 (top left), *Pan* 2 (bottom left), *Pan* 4 (top right), and *Pongo* (bottom right). Not to scale. The shape of the segments of these "androids" expresses their mass distribution, measured by the values of parameters k, a, b, and c, and, together with the density of each segment, allows prediction of the forces needed to bring about their individual motion. Addition of appropriate joint constraints, compliance, and damping allows forces to be predicted from motion for the rigid segment models as a whole.

TABLE 3. Mass proportions of the limb segments in hominoids

Code	TBM kg	Segment masses as percentage of TBM					
		Upper arm	Forearm	Hand	Thigh	Leg	Foot
Pongo 1	19.8	4.6	4.2	2.3	5.4	3.5	2.7
Pongo 2	27.8	3.7	3.2	1.2	4.7	2.3	1.8
Pongo 3	102.8	3.3	3.9	1.7	3.1	1.7	1.4
Variance		.443	.263	.303	1.39	.84	.443
Pan 3	4.0	3.4	2.7	1.0	5.2	2.6	1.4
Pan 1	33.1	3.9	2.8	1.0	6.8	2.7	1.7
Pan 2	47.1	4.5	3.5	1.3	7.9	2.9	1.5
Pan 4	57.1	4.5	3.6	1.4	7.6	3.6	1.4
Variance		.283	.217	.042	1.462	.203	.02
Child 1	28.8	3.4	1.7	.8	8.7	5.4	2.3
Child 2	39.3	3.2	1.3	.6	10.4	5.6	2.3
Child 3	40.7	3.5	1.8	.8	11.0	5.7	2.3
Human 1	50.4	3.0	1.6	.6	9.1	4.3	1.4
Human 2	58.0	2.9	1.7	.6	11.1	4.5	1.4
Human 3	58.3	3.0	1.7	.5	9.8	3.8	1.4
Human 4	58.5	3.1	1.8	.6	9.7	4.0	1.1
Human 5	76.0	2.7	1.6	.6	10.1	3.9	1.4
Human 6	89.0	2.6	1.7	.6	11.1	4.2	1.1
Variance		.88	.023	.10	.764	.575	.265
P. paniscus	29.5	3.6	3.3	1.0	7.2	3.5	1.4

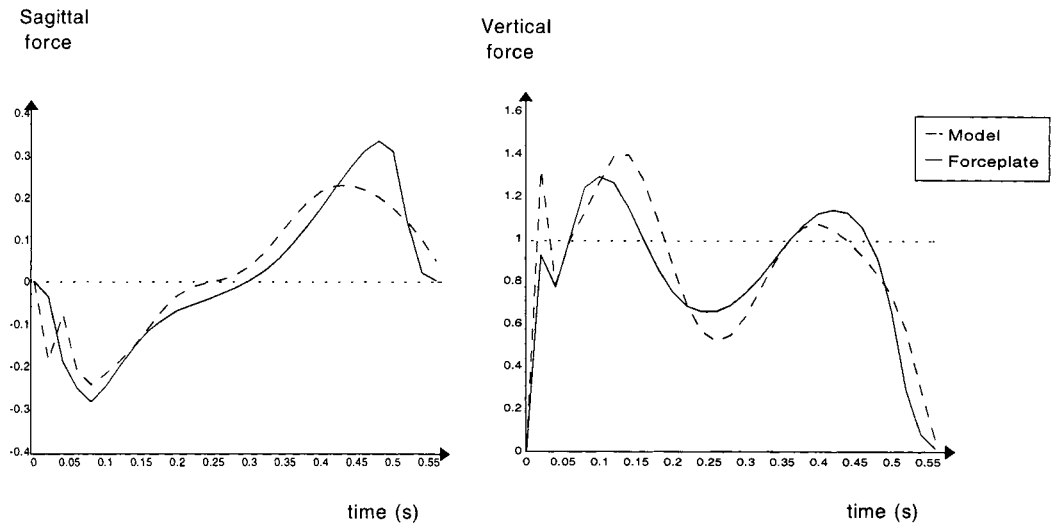

Fig. 5. Ground reaction forces (GRFs) measured by forece plate (solid lines) for subject LY compared to GRFs predicted from the same motion applied to an inertial model of the subject (dashed lines). Left, fore-aft force; right, vertical force.

is more likely to have been important for influencing posture and motion of the rest of the body during climbing and swinging than for any benefit in bipedal gaits. An equivalent effect to such proposed action of the larger moment of inertia during climbing and suspension is brought about by spinning ice-skaters, when they begin their spin with

extended arms, increasing the angular moment of the spin, then bring them progressively closer to the body. The larger the difference between the moment of inertia of the body in the two postures, the greater the spin speed achievable. For humans, pendular movement of the arms militates against a distal CG, not only as a distal CG would increase the resistance of the arm to swinging, but because a distal CG would make control, and fine-tuning of the pendular motion, very difficult.

We should also note that the single *Pan paniscus* specimen in our sample, from Zihlman (1988), was not notably different from our own *Pan troglodytes*. However, *Pan paniscus* has a higher leg mass ratio than our *P. troglodytes*. As in most of the former's segments, Zihlman's (1988) data show a higher leg mass ratio for the pygmy chimpanzee, which in this regard resembles Morbeck and Zihlman's (1988) small female *Pongo*, rather than humans. All the *P. paniscus* segment mass values fall within the range of our *P. troglodytes*, and we cannot offer any support for Zihlman's (1988) statement that *P. paniscus* has considerably heavier lower limbs than *P. troglodytes*. A greater sample size may of course confirm her finding.

Concerning the inertial models (Table 2), while the published data for *Macaca, Papio,* and *Lemur* are incomplete and are taken from different sources, the parameter *a*, which describes body shape, is uniform for these three non-hominoids. They are either in contrast to the hominoids as a whole, as is the case for the upper arm and thigh, or agree with other apes but differ from humans, as is the case for the leg. Further, it is noteworthy that the adult male chimpanzee, *Pan* 4, has the opposite sign for the parameter *a* to the majority of other hominoid specimens, reflecting the very robust build of this individual. Such robusticity is probably largely attributable to sexual dimorphism, since the other hominoids we measured were either subadult or female. The parameter is thus an effective tool in indicating gracility or robusticity of body form.

While the graphical representations of the inertial parameters (Fig. 4) may not appear morphologically similar to the original specimens, they are accurate representations of the distribution of mass along the segments. They are, within the limits of our technique, an accurate reflection of the differences in mass distribution between the subjects. They highlight differences such as that in robusticity between the individuals of *Pan,* and the very distinct cranial shape of the infant *Pongo*. Given that density is the same, solid models of the segments of the shape shown in Figure 4 will have the same biomechanical properties as the actual segments which they represent. Further, given appropriate joint constraints, compliance, and damping, a link-segment model comprising such modelled segments will behave mechanically in the same manner as the individual it represents. Evidence for this claim appears in Figure 5, which compares real and simulated ground reaction forces in the vertical and sagittal (fore-aft) directions for one of us (LY) walking at normal speed. For the vertical force, our force plate record, and the record calculated by dynamic modelling, show three peaks. The first is the so-called "heel-strike transient," which is a common, but not universal feature of normal human gait (Whittle, 1993). In the real record, the transient reaches a force of about 1 × body weight (BW), but the fact that the calculated force reaches about 1.3 × BW suggests the model does not model heel-strike particularly well. The simulated record then rises to a second peak of about 1.3 × BW during full-foot, while the foreceplate registers a peak of 1.4 × BW, and then both fall off during mid-stance to heel-off, the simulation to 0.55 × BW, the forceplate record to 0.7 × BW, before both rise to a final peak of about 1.15 × BW during heel-off. The calculated fore-aft force again shows a similar overall pattern, and the magnitude of the fore-force at heel-strike is reasonably similar to the measured force, but the calculated aft force is lower. Thus, the model simulates the pattern of forces well, but the magnitude of the peaks and troughs in the calculated forces is not always the same, and their phase is in some places delayed. The difference almost certainly indicates that a rigid-link model, as a simplified representation of the properties of a real body, will always tend to be less compliant and less well damped than is a real human, even if compliant ele-

ments and damping are introduced in the model's joints. However, elsewhere (Crompton and Li (in press) we have shown that the vertical and sagittal forces produced by simulations of slow, normal, fast, and chimp-like bipedal walking fall within the range of variation of the equivalent forces produced by real humans performing the same activity, in a plot of the performances against the first three principal components of the Fourier coefficients of the force curves. Thus, dynamic modelling can indeed adequately predict forces operating in the real world mechanics of human bipedal gaits.

CONCLUSION

We have sought in this paper to present a method for measurement, representation, and comparison of the mass and inertial properties of the body segments that is optimised for utility in biomechanical analysis of primate locomotion, but capable of being carried out using simple laboratory equipment on the less-than-ideal specimens which are generally available from natural zoo death and autopsy. Further, our modelling technique allows the same data to be derived from simple linear measurements of precious museum specimens or living individuals, even under field conditions. The accuracy of our method is indicated by our ability to simulate the pattern of the external reaction forces of bipedal walking in a real individual from knowledge of motion and mass distribution of the subject, although a tendency for simulations to behave more rigidly than real musculoskeletal systems was observed. We have also been able to confirm some, but not all, of the predictions made by Preuschoft and Witte (1991) on theoretical grounds. While our detailed findings on the mechanics of hominoid and early hominid locomotion have been and will be published in other papers (Crompton and Li (in press)); we hope that by demonstrating the utility of these techniques, we will encourage other primatologists to study segment mass properties as readily as they now gather support orientations, heights, and frequencies of locomotor modes. The former are at least as important as the latter to an understanding of primate and human locomotor evolution.

ACKNOWLEDGMENTS

We thank the North of England Zoological Society for its continued hospitality to our research. This research is funded by the National Environment Research Council, the Biotechnology and Biological Sciences Research Council, the Medical Research Council, the Ema and Victor Hasselblad Foundation, and Tektronix Inc.

LITERATURE CITED

Bresler B and Frankel JP (1950) The forces and moments in the leg during level walking. Trans. ASME *72*:27–36.

Cavagna GA, Heglund NC, and Taylor CR (1977) Mechanical work in terrestrial locomotion: Two basic mechanisms for minimizing energy expenditure. Am. J. Physiol. *23*:233–261.

Chandler RF, Clauser CE, McConville JT, Reynolds HM, and Young JW (1975) Investigation of inertial properties of the human body. Aerospace Medical Research Laboratory document AMRL-TR-74-137. Ohio: Wright-Patterson Air Force Base.

Clauser CE, McConville JT, and Young JW (1969) Weight, volume, and center of mass of segments of the human body. Aerospace Medical Research Laboratory document AMRL-TR-69-70. Ohio: Wright-Patterson Air Force Base.

Contini R (1972) Segment parameters—Part II. Artificial Limbs *16*:1–19.

Crompton RH, Sellers WI, and Günther MM (1993) Energetic efficiency and ecology as selective factors in the saltatory locomotion of prosimian primates. Proc R. Soc. Lond. [Biol.] *254*:41–45.

Crompton RH, Li Y, (in press) Running Before They Could Walk? Locomotion, Adaptation and Bipedalism in Early Hominids. In: JAJ Gowlett: Archaeological Sciences, Oxford: Oxbow Press.

Demes B and Gunther MM (1989) Biomechanics and allometric scaling in primate locomotion and morphology. Folia Primatol. *53*:125–141.

Dempster WT (1955) Space requirements of the seated operator. Aerospace Medical Research Laboratory WADC technical report 55 159. Ohio: Wright-Patterson Air Force Base.

Grand TI (1977a) Body weight: Its relation to tissue composition, segment distribution, and motor function. I: Interspecific comparisons. Am. J. Phys. Anthropol. *47*:211–240.

Grand TI (1977b) Body weight: Its relation to tissue composition, segment distribution, and motor function. II: Development of *Macaca mulatta*. Am. J. Phys. Anthropol. *47*:241–248.

Hanavan EP (1964) A mathematical model of the human body. Aerospace Medical Research Laboratory document AMRL-TR-64-102. Ohio: Wright-Patterson Air Force Base.

Harless E (1860) The static moments of the component masses of the human body. Reprinted in Aerospace Medical Research Laboratory document FTD-TT-1-295 (1962). Ohio: Wright-Patterson Air Force Base.

Haug EJ (1989) Computer-Aided Kinematics and Dynamics of Mechanical Systems. Vol. 1: Basic Methods. Massachusetts: Needham Heights: Allyn and Bacon.
Hildebrand M (1985) Walking and running. In M Hildebrand, DM Bramble, KF Liem, and DB Wake (eds.): Functional Vertebrate Morphology. Cambridge, Mass.: Harvard University Press, pp. 3–57.
Jenkins FA Jr (1972) Chimpanzee bipedalism: Cineradiographic analyses and implications for the evolution of gait. Science *178*:877–879.
Jensen RK (1978) Estimation of the biomechanical properties of three body types using a photogrammetric method. J. Biomech. *11*:349–358.
Li Y (1991) Ontogeny of children's limbs, with particular reference to inertial characteristics. Unpublished PhD dissertation, University of Liverpool.
Li Y and Dangerfield PH (1993) Inertial characteristics of children and their application to growth study. Ann. Hum. Biol. *20*:433–454.
MDI, Mechanical Dynamics, Inc. (1992) ADAMS, Version 6.1. Ann Arbor, Mich.
Mochon S and McMahon TA (1980) Ballistic walking. J. Biomech. *13*:49–57.
Morbeck ME and Zihlman AL (1988) Body composition and limb proportions. In JH Schwartz (ed.): Orang-Utan Biology. Oxford: Oxford University Press, pp. 285–297.
Peters A and Preuschoft H (1984) External Biomechanics of Leaping in *Tarsiers* and its Morphological and Kinematic Consequences. In C Niemitz (ed.): Biology of Tarsiers. New York: Gustav Fischer, pp. 227–256.
Preuschoft H and Witte H (1991) Biomechanical reasons for the evolution of hominid body shape. In Y Coopens and B Senut (eds.): Origine(s) de la Bipedie chez les Hominidés. Paris: Editions du CNRS, pp. 59–78.
Preuschoft H, Witte H, and Demes B (1992) Biomechanical factors that influence overall body shape of apes and humans. In S Matano, RH Tuttle, H Ishida, and M Goodman (eds.): Topics in Primatology: Vol. 3. Evolutionary Biology, Reproductive Endocrinology and Virology. Tokyo: University of Tokyo Press, pp. 259–289.
Reynolds HM (1974) Measurement of the inertial properties of the segmented savannah baboon. PhD dissertation, Southern Methodist University.
Santschi WA, DuBois J, and Omoto CE (1963) Moments of inertia and centers of gravity of the living human body. Aerospace Medical Research Laboratory document AMRL TDR-63-36 Ohio: Wright-Patterson Air Force Base.
Sellers WI (1992) A study of leaping in prosimian primates. Unpublished PhD dissertation, University of Liverpool.
Sellers WI and Crompton RH (1994) A system for 2- and 3-D kinematic and kinetic analysis of locomotion, and its application to analysis of the energetic efficiency of jumping in prosimians. Zeits. Morph. Anthropol. *80*:99–108.
Steidel RF (1967) Mechanics of solids. In T Baumeister (ed.): Marks' Standard Handbook for Mechanical Engineers. New York: McGraw Hill, pp. 3.2–3.32.
Tardieu C (1991) Etude comparative des deplacements du centre du gravite du corps pendant la marche par une nouvelle methode d'analyse tridimensionelle. Mise a l'epreuve d'une hypothese evolutive. In Y Coppens and B Senut (eds.): Origine(s) de la Bipedie chez les Hominidés. Paris: Editions du CNRS, pp. 49–58.
Tardieu C (1992) Le Centre de Gravite Du Corps et sa Trajectorie pendant la Marche. Paris: Editions du CNRS.
Tardieu C, Aurengo A, and Tardieu B (1993) New method of three-dimensional analysis of bipedal locomotion for the study of displacements of the body and body parts centers of mass in man and non-human primates: Evolutionary framework. Am. J. Phys. Anthropol. *90*:455–476.
Vilensky JA (1979) Masses, centers-of-gravity, and moments-of-inertia of the rhesus monkey. Am. J. Phys. Anthropol. *50*:57–66.
Whittle M (1993) Gait Analysis: An Introduction. Oxford: Butterworth-Heinemann.
Wells JP and DeMenthon DF (1987) Gravity and determination of moments of inertia by double pendulum in *Lemur fulvus*. Am. J. Primatol. *12*:299–308.
Winter DA (1990) Biomechanics and Motor Control of Human Movement. New York: Wiley.
Yamazaki N, Ishida H, Kimura T, and Okada M (1979) Biomechanical analysis of primate bipedal walking by computer simulation. J. Hum. Evol. *8*:337–350.
Zihlman AL (1984) Body build and tissue composition in *Pan paniscus* and *Pan troglodytes* with comparisons to other hominoids. In RL Susman (ed.): The Pygmy Chimpanzee. New York: Plenum, pp. 179–200.

APPENDIX A: MATHEMATICAL METHOD FOR CALCULATION OF INERTIAL PARAMETERS

Following Steidel (1967), the moment of inertia I_2, of the frame/specimen assembly about axis 2 (Fig. 3) will be given by Equation 1.

$$I_2 = \frac{mgd_2}{(2\pi f_2)^2} \tag{1}$$

where m is the mass of the frame/specimen assembly, g the gravitational acceleration, and f_2 the frequency of its swing about axis 2. In order to obtain from this the moment of inertia about the center of gravity I_0 we apply the parallel axis theorem:

$$I_0 = \frac{mgd_2}{(2\pi f_2)^2} - md_2^2 \tag{2}$$

A similar equation for I_0 can be set up considering swinging about axis 1. Equating the two expressions for I_0:

$$\frac{mgd_1}{(2\pi f_1)^2} - md_1^2 = \frac{mgd_2}{(2\pi f_2)^2} - md_2^2 \tag{3}$$

where f_1 is the frequency of swing about axis 1 and d_1 is the distance between axis 1 and

the center of gravity of the assembly. Again with reference to Figure 2:

$$d_1 = d + d_2 \tag{4}$$

and by solving Equations 3 and 4 simultaneously:

$$d_2 = \frac{df_2^2(g - 4\,d\pi^2 f_1^2)}{-gf_2^2 + 8d\pi^2 f_1^2 f_2^2 + gf_1^2} \tag{5}$$

Equation 5 above is used to locate the center of gravity of the assembly, S_y, and then Equation 1 above is used once again to calculate the moment of inertia about axis 2.

The same method, applied to the empty frame, gives the moment of inertia of the frame about axis 2, $I_{f,2}$, and the distance of the frame's center of gravity from axis 2, $d_{f,2}$. The moment of inertia of the specimen alone about axis 2 is given by:

$$I_{s,2} = I_2 - I_{f,2} \tag{6}$$

and the distance of the center of gravity of the specimen from axis 2, $d_{s,2}$ is:

$$d_{s,2} = \frac{d_2 m - d_{f,2} m_f}{m_s} \tag{7}$$

where m_f is the mass of the frame and m_s the mass of the specimen. By applying the parallel axis theorem again we find the principal moment of inertia $I_{s,0}$ of the segment (the principal moment of inertia is the moment of inertia about the center of gravity):

$$I_{s,0} = I_{s,2} - m_s d_{s,2}^2 \tag{8}$$

Finally, the radius of gyration, r_s, of the segment is obtained from:

$$r_s = \sqrt{\frac{I_{s,0}}{m_s}} \tag{9}$$

Most limb segments can safely be assumed to have equal moments of inertia and radii of gyration in the v and u directions but this is not so for the trunk and hands, and in these cases, therefore, we swung these specimens in two orthogonal planes to derive the inertial properties in each direction. The feet of these specimens were judged likely to have very similar inertial values in the two directions, and only one value is given.

Method for the trunk

In the case of the trunk, exactly the same technique could be applied, but we did not have the technical facilities to build an equally accurate frame of adequate size, and a different method was adopted. A balance-board technique derived from Contini (1972) was employed to derive the location of the center of gravity with reference to the center of the acetabulum. Then, the torso is frozen and two holes are drilled through the pelvis at right angles. A strong stainless-steel rod is passed through each hole in succession and the moment of inertia determined for the v and u planes by a single set of swings in each direction.

The moment of inertia I of the segment about the rod is:

$$I = \frac{WL}{4\pi^2 f^2} \tag{10}$$

where L is the distance of the center of gravity of the specimen to the rod. The principal moment of inertia is then:

$$PMI = I - \left(\frac{W}{g}\right)L^2 \tag{11}$$

(Dempster, 1995).

Correction for the trunk data in eviscerated specimens

It is usually the case that specimens are obtained from zoo collections after autopsy, and that the viscera are thus not intact when the cadaver is received. Therefore, we have developed a method of correction for the removal of abdominal and thoracic viscera. Among the four chimpanzees and one orang dismembered in our laboratory, one male (*Pan* 4) and one female chimpanzee (*Pan* 1) had entire internal organs in their trunks when the work was undertaken. The trunk data of the other three, eviscerated individuals could thus be corrected for on the basis of the two intact individuals (bearing in mind the difficulty of applying the proportions of *Pan* to *Pongo*). The inertial properties of the trunk of *Pan* 1 were measured

three times (whole trunk, trunk with abdominal organ removed, and trunk with viscera removed), and these data were then used to calculate the trunk parameters of *Pan* 2, *Pan* 3, and the single *Pongo*.

For mass, it has been assumed that the mass ratio of the trunk without internal organs, (T'), over the intact trunk is the same in each individual. Based on this assumption, there is a relationship:

$$\frac{T'_{PAN1}}{T_{PAN1}} = \frac{T'_{Other}}{T_{Other}} \tag{12}$$

For the center of gravity, we assumed that the distance between the center of gravity of the internal organs (CG') and the hip joint in ratio to the trunk length is the same in each individual. This ratio was estimated, on the basis of *Pan* 1, as 40.8%. Then from the relationship:

$$M_1 CG_1 + 0.408\, M_2 = M \times CG \tag{13}$$

where M_1 is the mass of the trunk without internal organs, CG_1 is the center of gravity of the trunk without the internal organs, and M_2 is the mass of the internal organs themselves, the center of gravity (CG) of the trunk in question can be calculated.

For the radius of gyration (RG), the situation is more complicated, and no logical relation can be derived. We thus had to assume that the ratio of the RG of the whole trunk over the RG of the trunk without the internal organs was the same in all specimens as it was in *Pan* 1.

Method of constructing models

We then first create a column-shaped model (Fig. 1). Each cross section of the column is an ellipse, and the long axis of the ellipse is:

$$u = \sqrt{az^2 + bz + c} \tag{14}$$

where z is the height of the given cross section and its short axis:

$$v = ku \tag{15}$$

For example, in a bar of length 0.25 m, diameter 0.06 m, and mass density 1 g/cm^3, its center of gravity will be exactly half-way along (50% of its length), its radius of gyration will be 29.5% of its length, and its mass 0.707 kg. Parameters a, b, c, and k will have the following values: $a = 0$, $b = 0$, $c = 0.03^2 = 0.0009$, and $k = 1$. It can be mathematically modelled:

$$u = \sqrt{c} \tag{16}$$

Then if there is a segment with length = 0.25 m, radius of gyration 31.7% of its length, its center of gravity located at 51.4% of its length, starting from its proximal end, and a mass of 3.4 kg, we can model it by a solid of revolution (Fig. 1A) with the same length, a base diameter of 0.04 m and a radius at a given point of:

$$\sqrt{0.003\, z + 0.004} \tag{17}$$

where z is the distance from the point to the base plane. In this case $k = 1$, $a = 0$, $b = 0.003$, and $c = 0.004$.

In the most complete case, when parameter $a \neq 0$, the outline of the solid of revolution can be either convex or concave. If $a < 0$, the outline is more likely to be convex (Fig. 1A), representing a smaller radius of gyration, but if $a > 0$, the outline is concave, representing a larger radius of gyration. For segments of circular cross section, the mass of the segment is then:

$$\begin{aligned} m &= \pi\rho \int_0^L q^2 dz = \pi\rho \int_0^L (az^2 + bz + c) \\ &= \pi\rho \left(\frac{1}{3} aL^3 + \frac{1}{2} bL^2 + cL\right) \end{aligned} \tag{18}$$

where ρ is the mass density and L the segment length, and q is the radius of the solid

of revolution. The center of gravity along the z axis is then:

$$cg = \frac{\int_0^L zq^2dz}{\int_0^L q^2dz} = \frac{1}{2}\frac{3aL^2 + 6c + 4bL}{6c + 3bL + 2aL^2} \quad (19)$$

The moment of inertia of the segment is:

$$MI = \rho\pi \int_0^L (0.25q^4 + z^2q^2)dz \quad (20)$$

and the moment of inertia about the center of gravity (that is, the principal moment of inertia, PMI) is:

$$PMI = MI - cg^2m \quad (21)$$

and the radius of gyration can be derived using Equation 9. Then, there is a relationship:

$$cr = cg^2 + rg^2 = \frac{MI}{m} = \frac{10b^2L^2 + 30c^2 + 24aL^4 + 30bL^3 + 40cL^2 + 15abL^3 + 20acL^2 + 6a^2L^4 + 30bcL}{20(6c + 3bL + 2aL^2)} \quad (22)$$

Solving these simultaneous equations about m, CG, and cr gives us the values of a, b, and c. The parameters for the elliptical cross section model are obtainable in a similar way. In this case, there are four unknown variables in the equation groups, namely a, b, c, and k, which are to be calculated from m, CG, cr_{vv}, and cr_{uu}. Thus, if the parameter a in an equation is positive, the model will have a relatively large radius of gyration, and vice versa. If both a and b are zero, the model is a column with radius equal to the square root of c. The square root of c also represents the radius of the proximal end of a model with any given value for a and b.

Estimation of mass distribution in intact and/or living specimens

While inertial properties can always be most accurately determined by dissection techniques, the properties of segments may also be derived non-invasively, since the curve u in Equation 14 may be estimated by measuring the diameter of circular segments or, should the segment appear elliptical, the long and short diameters, at a minimum of three locations of known distance along the segment, and fitting a curve to their radii, as shown in Figure 1A. For a limb segment such as upper arm or forearm, where the cross section tends to be circular in primates, the inertial properties can be estimated (using with the model) by seven linear measurements. By measuring the values of diameters z_1, and u_1, z_2, and u_2, z_3, and u_3, and length L, the model parameters a, b, and c can be estimated, for each curve as:

$$a = \frac{z_1u_3^2 - z_3u_1^2 - z_2u_3^2 - z_1u_2^2 + z_2u_1^2 + z_3u_2^2}{p} \quad (23)$$

where the dummy variable p is:

$$p = z_1z_3^2 - z_2z_3^2 + z_2z_1^2 - z_3z_1^2 + z_3z_2^2 - z_1z_2^2 \quad (24)$$

$$b = \frac{z_1^2u_3^2 - z_1^2u_2^2 - z_3^2u_1^2 + z_2^2u_2^2 - z_2^2u_3^3 + u_1^2z_2^2}{p} \quad (25)$$

and

$$c = \frac{-u_1^2z_2z_3^2 + z_2^2z_3u_1^2 + z_1^2z_2u_2^2 - z_2^2z_3u_3^2 + u_2^2z_1z_3^2 - z_2^2z_1u_3^2}{p} \quad (26)$$

If the segment is elliptical, k is estimated as the mean of the ratios of the radii in the v and u direction at each cross section (v_1/u_1, v_2/u_2, and v_3/u_3). If it is circular, $k = 1$. From the parameters a, b, c, and k and the measurement L, we can calculate the inertial characteristics of any segment with an elliptical or circular cross section:

$$\text{Mass} = \frac{1}{6}\rho\,\pi\,kL\,(3bL + 6c + 2aL^2) \quad (27)$$

$$\text{Center of gravity} = \frac{1}{2}\frac{4bL + 6c + 3aL^2}{3bL + 6c + 3aL^2} \quad (28)$$

Moment of inertia of v-v axis

$$= \rho\pi\left(\frac{1}{12}kb^2L^3 + \frac{1}{3}kcL^3 + \frac{1}{20}ka^2L^5 + \frac{1}{4}kc^2L + \frac{1}{6}kcaL^3 + \frac{1}{5}kaL^5 + \frac{1}{4}kbL^4 + \frac{1}{4}kcbL^2 + \frac{1}{8}kbaL^4\right) \quad (29)$$

Moment of inertia of u-u axis

$$= \rho\pi\left(\frac{1}{3}kcL^3 + \frac{1}{20}k^3a^2L^5 + \frac{1}{5}kaL^5 + \frac{1}{4}kbL^4 \right. \quad (30)$$

$$\left. + \frac{1}{6}k^3caL^3 + \frac{1}{8}k^3baL^4 + \frac{1}{12}k^3b^2L^3 + \frac{1}{4}k^3cbL^2 + \frac{1}{4}k^3c^2L\right)$$

where ρ is a suitable value for the density of the segment. Values could be substituted for each segment from the figures in Table 1, if no cadavers at all are available. The sum of all segment masses should be course closely approximate the weighed mass of the animal!

APPENDIX B: FORTRAN 90 SOURCE CODE FOR CALCULATION OF INERTIAL PROPERTIES OF LIVING SUBJECTS

NB: This program assumes $z_1 = 0$, $z_2 = L/2$ and z3 = L. It must be compiled exactly as is, with the present layout and spacing. We cannot offer support to users of this code, nor can we accept any responsibility for any consequences of its use. Any publications from research using this code, or a subset of this code, should of course cite the present publication, and we should appreciate a reprint of the published paper.

```
      Programme Inertia
c     Measurements entered must be in mm
c     This programme complies with the FORTRAN 90 standard
      dimension zl(19,99),dia(19,99,3),t(99,2),aa(19,99),bb(19,99)
      dimension am(99),sk(19,99),cc(19,99)
      real l,m(19,99),cg(19,99),rg(19,99,2),k,mass,mixx,miyy
      parameter(pi=3.1416)
c     Input file name: seg
c     Output file name: results
      open(1,file='seg')
      open(2,file='results')
c     n_sub: Number of subjects; n_seg: Number of segments
c     Input file data format:
c     Each segment has a block of data, which includes the measurements
c       for the same segment in  all subjects

c  n_sub n_seg
c    L1  L2  ...     Ln_sub                    (Lj :Length for subject j)
c    Px1 Py1  Px2 Py2 ...  Pxn_sub Pyn_sub     (P: Proximal |x/y:Diameter in)
c    Mx1 My1  Mx2 My2 ...  Mxn_sub Myn_sub     (M: Middle   |  direction of )
c    Dx1 Dy1  Dx2 Dy2 ...  Dxn_sub Dyn_sub     (D: Distal   |  x or y       )
c                                          (Dx1:Distal diameter of the segment
c                                             of subject 1 at x axis)
c    Px1 Py1  Px2 Py2 ...  Pxn_sub Pyn_sub
```

```
c     Mx1 My1  Mx2 My2 ...  Mxn_sub Myn_sub      (The second segment)
c     Dx1 Dy1  Dx2 Dy2 ...  Dxn_sub Dyn_sub
c
c     Px1 Py1  Px2 Py2 ...  Pxn_sub Pyn_sub
c     Mx1 My1  Mx2 My2 ...  Mxn_sub Myn_sub      (The third segment)
c     Dx1 Dy1  Dx2 Dy2 ...  Dxn_sub Dyn_sub
c
c        ..................
c
c
        read(1,*) n_sub, n_seg
        do 1 i=1,n_seg
        do j=1,n_sub
                sk(i,j)=0
        end do
        read(1,*) (zl(i,j),j=1,n_sub)
        do j=1,n_sub
                zl(i,j)=zl(i,j)/10.
        end do
        do mm=1,3
                read(1,*) ((t(j,kk),kk=1,2),j=1,n_sub)
                do j=1,n_sub
                        sk(i,j)=sk(i,j)+t(j,2)/t(j,1)
                        dia(i,j,mm)=t(j,1)/2.
                end do
        end do
        do j=1,n_sub
                sk(i,j)=sk(i,j)/3
        end do
1       continue
```

```
      do 21 i=1,n_seg
      do 21 j=1,n_sub
      l=zl(i,j)
      y1=dia(i,j,1)**2
      y2=dia(i,j,2)**2
      y3=dia(i,j,3)**2
      cc(i,j)=y1
      aa(i,j)=-2/l**2*(2.*y2-y1-y3)
      bb(i,j)=(-y3+4.*y2-3*y1)/l
      c=cc(i,j)
      b=bb(i,j)
      a=aa(i,j)

      k=sk(i,j)
      t4 = l**2
      mass = pi*k*l*(3*b*l+6*c+2*a*t4)/6
      m(i,j)=mass

      t1 = b*l
      t3 = 6*c
      t4 = l**2
      t5 = a*t4
      cg(i,j) = l*(4*t1+t3+3*t5)/(3*t1+t3+2*t5)/2
      t1 = l**2
      t2 = t1**2
      t5 = k**2
      t6 = c*t1
      t10 = c**2
      t18 = b*t1*l
      t23 = a**2
      t27 = b**2
      mixx=k*pi*l*(24*a*t2+20*a*t5*t6+30*t10*t5+30*c*t5*b*l+
     $  15*a*t5*t18+30*t18+6*t5*t23*t2+10*t27*t5*t1+40*t6)/120
```

```
      t1 = b**2
      t2 = l**2
      t5 = c**2
      t7 = a**2
      t8 = t2**2
      t12 = b*t2*l
      t20 = c*t2
      miyy=k*pi*l*(10*t1*t2+30*t5+6*t7*t8+15*a*t12+30*c*b*l+
     $    24*a*t8+20*a*t20+30*t12+40*t20)/120
      rg(i,j,1)= sqrt((mixx-cg(i,j)**2*m(i,j))/m(i,j))/l*100.
      rg(i,j,2)= sqrt((miyy-cg(i,j)**2*m(i,j))/m(i,j))/l*100.
      cg(i,j)= cg(i,j)/l*100.
21    continue
      write(2,18)
      write(2,'(80(1H_))')
      do 41 i=1,n_seg
      write(2,*) 'Segment No.',i
      do j=1,n_sub
        write(2,8) sk(i,j),zl(i,j),m(i,j),cg(i,j),rg(i,j,1),rg(i,j,2),
     $       aa(i,j),bb(i,j),cc(i,j)
      end do
      write(2,*) ' '
41    continue
      write(2,'(80(1H_))')
      write(2,*) ' '
      write(2,*) ' '
      write(2,*)'  K:      The ratio of the diameters of y/x for the m
     1odel'
      write(2,*)'  Length: Length of the segment model, same as the in
     1put'
      write(2,*)'  Mass:   Mass of the model, an estimation for the li
     1mb segment'
```

```
      write(2,*)'  CG:      Centre of mass along the long (z) axis'
      write(2,*)'  RGxx:    Radius of gyration for xx plane'
      write(2,*)'  RGyy:    Radius of gyration for yy plane'
      write(2,*)'  a:       Parameter a in model v=sqrt(a*u*u+b*u+c)'
      write(2,*)'  b:       Parameter b in model v=sqrt(a*u*u+b*u+c)'
      write(2,*)'  c:       Parameter c in model v=sqrt(a*u*u+b*u+c)'

 8    format(2x,f7.4,f7.1,f9.2,3f8.2,4x,f11.7,f8.3,f6.2)
18    format(2x,7H      K,7H Length,9H     Mass,8H      CG,8H    RGxx,
     1  8H    RGyy,4x,11H          a,8H       b,6H     c)
      end
```